HEFAT2010
7th International Conference on Heat Transfer, Fluid Mechanics and Thermodynamics
19-21 July 2010
Antalya, Turkey

A NUMERICAL STUDY ON THE FLUID STRUCTURE INTERACTION OF A TRANSONIC AXIAL COMPRESSOR WITH INLET GUIDE VANE

Ko S.H.*, Yang, S.S., Kang Y.S., Han S.Y. and Kim Y.T.
Department of Mechanical Design Engineering,
Chungnam National University
Daejeon,
South Korea
E-mail: sunghoko@cnu.ac.kr

ABSTRACT

The present study describes the effects of IGV(inlet guide vane) on the internal flow of the rotor blades of a transonic axial compressor. Numerical solutions of the governing RANS equations for the three dimensional turbulent flows inside the compressor have been obtained by utilizing the ANSYS CFX program. The assessment of the IGV's aerodynamic performance has been made by analyzing the CFD solutions of compressor and some calculated flow characteristics such as isentropic efficiency, total pressure, static pressure, incidence angle, and Mach number. Furthermore, a fully-coupled fluid structure interaction(FSI) analysis for the rotor has been made by utilizing both CFD and FEM solver of the ANSYS CFX program.

INTRODUCTION

The blades of aircraft jet engine under extreme operating conditions suffer from damages such as creep, stress fracture, oxidation corrosion, long-term fatigue, short-term fatigue and thermal-stress. As for the rotating blades of the compressor, incidence angle has been known to be a major cause for these damages. Therefore, it is necessary to investigate the effects of incidence angle on three-dimension flow and pressure loss inside the compressor in order to obtain high efficiency and high performance of the jet engine.

The main function of the IGV is to provide constant flow angle to rotor blades regardless of climate, flight velocity and other operating conditions, which extends operating band of the engine. The IGV, also, is utilized to delay shock formation in the compressor by reducing relative Mach number of inlet air and to reduce incidence angle of the rotor at low flow rate condition.[1] Chae and Lee[2] studied effects of incidence angle on the three-dimensional flow and aerodynamic loss downstream of a high-turning turbine rotor blade.

Internal flow of the transonic axial compressor has complex three dimensional flow structure due to secondary flow, wake, shock wave and others from a blade shape.[3] During past two decades many CFD methods have been developed and used for predicting these complex flow characteristics of the compressor. Nowadays commercial program becomes a general rule of the designing tool for the high-efficiency turbine machine because of its convenient graphic user interface.

The main objective of the present study is to assess the IGV by calculating the vibration and flow characteristics of the rotor blades of the transonic axial multi-stage compressor. A commercial program is utilized to conduct the FSI of the rotor blades by carrying out FEM analysis as well as CFD calculation simultaneously.

NUMERICAL METHOD

Figure 1 shows the meridional view of the three-stage transonic axial compressor which is under development by Korea Aerospace Research Institute(KARI). The compressor constitutes one row of the IGV followed by three rotor-stator stages. Since the effects of the IGV are limited mainly on the first stage, the present numerical study analyzed only the first stage of the compressor. The AxCent program was used to create the modeled three dimensional geometry of the first stage of the compressor with IGV shown in Figure 2.

Table 1 provides the basic specification of the compressor. The compressor has the mass flow rate of 9.8kg/s and rotates at 20,000 rpm. The IGV row has 41 blades and there are 26 rotor blades and 47 stator blades in the first stage.

The multi-block grid system of compressor is based on O-H mapping created by ANSYS CFX-Turbogrid program. Grids of

inlet, outlet and the blade passage are H-type grids, and grids around the blade are O-type grids. The rotor blade has tip clearance of 5mm and a H-type grid was employed to fill the clearance. The numbers of grid points in the IGV, rotor and stator blocks, shown in Figure 3, are 110,000, 100,000, and 100,000, respectively. Numerical analysis of the compressor has been made for one flow passage of the compressor by assuming the flow inside the compressor is uniformly periodic in the circumferential direction.

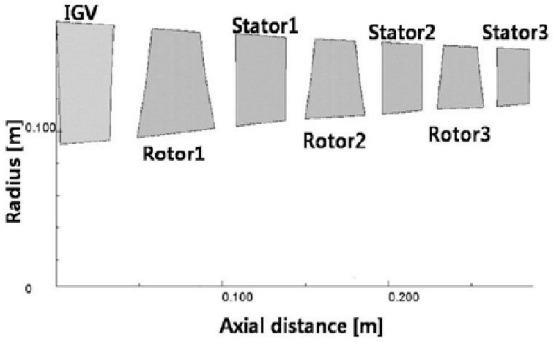

Figure 1 Meridional view of a three-stage transonic axial compressor with IGV

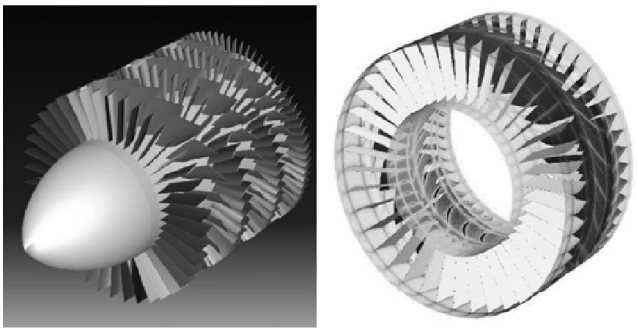

(a) Full model (3 stages) (b) analysis model (1st stage)

Figure 2 Modeling of the first stage of the axial compressor

Table 1 Basic conditions of the first stage of the compressor

Number of Blades	IGV	41Ea
	Rotor	26 Ea
	Stator	47 Ea
Inlet Condition	Total Pressure	101,325 Pa
	Total Temperature	288 K
Mass Flow rate		9.8 kg/s
RPM		20,000 rpm

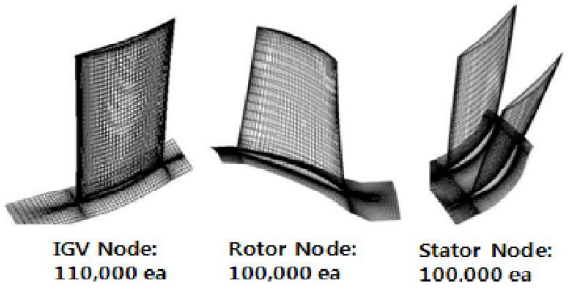

Figure 3 Surface mesh of IGV, rotor and stator

Figure 4 summarizes the boundary conditions applied to the computational domain. Total pressure and total temperature are specified at the inlet of the domain. The outlet of the domain has a specified static pressure which is given by the system designer of the compressor. The interfaces between the rotating block and the stationary blocks have the 'frozen rotor' boundary condition. The no-slip boundary condition is applied to all the solid surfaces including the blades, the hub, and the shroud. The sides of the domain have the periodic boundary condition.

Figure 5 and 6 show the variation of the cross sectional profiles the IGV and rotor blade from hub to tip. The stationary IGV shows little variation of the blade angle from hub to tip meanwhile the trailing edge of the rotor blade shows about 50 degree twisting from hub to tip to accommodate the speed variation due to rotation.

The CFD solver utilized the standard k-ε turbulence model with the wall function to evaluate the eddy viscosity of the flow field. Turbulence intensity at the inlet of the domain is specified

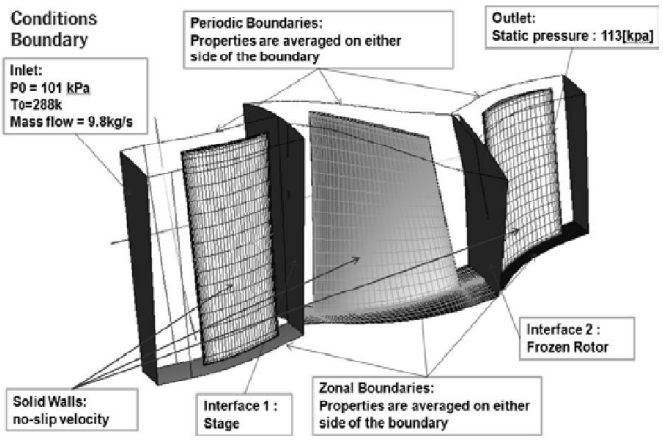

Figure 4 Computational domain and boundary conditions

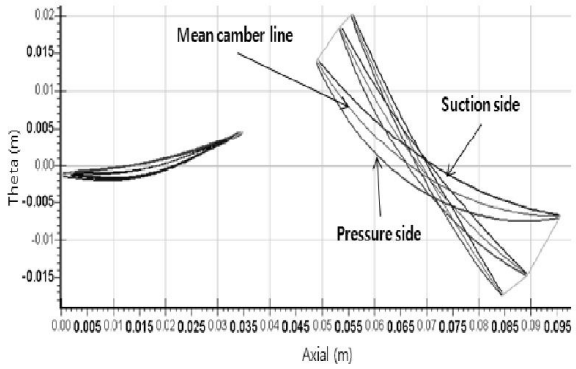

Figure 5 Cross sectional blade profiles of IGV and rotor

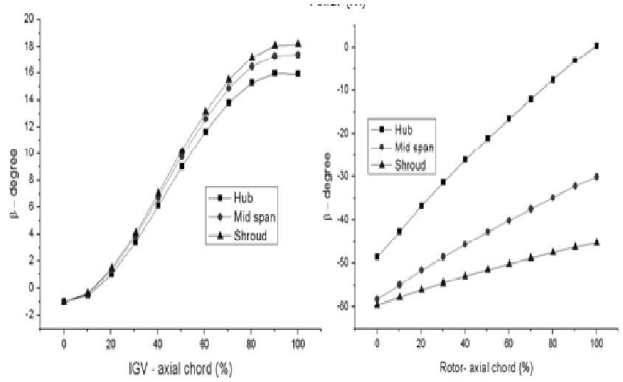

Figure 6 Distribution of the blade angle of IGV and rotor

CFD ANALYSIS

A steady-state CFD solution is obtained to assess the aerodynamic performance of the first stage of the compressor. The CFD solution will be used as the initial flow field of the FSI computation.

Table 2 shows the CFD solution for the performance of the KARI compressor operating at design point. The flow coefficient is defined as the rate between axial velocity and rotational velocity of the mean. In the present case, the flow coefficient is 0.49 at the inlet of the rotor and 0.51 at the outlet of the rotor. Despite the decrease in volume by the pressure rise, the flow is accelerated in the axial direction mainly due to the reduction of the flow passage area. The isentropic efficiency of the first stage is close to the polytropic efficiency of the compressor, which is calculated to be 0.86.

Table 2. Computed results for the compressor operating at design point

Performance	Computed Results
Inlet flow coefficient	0.49
Outlet flow coefficient	0.51
Total pressure ratio	1.38
Total temperature ratio	1.1
Isentropic efficiency	86.1%
Polytropic efficiency	86.6%

Figure 7 shows distribution of the averaged total pressure inside the first stage of the compressor. In the figure, the x-axis is labeled as 0~1(IGV), 1~2(rotor), and 2~3(stator), and the y-axis shows total pressure variation. As the flow passes through the IGV, the total pressure decreases a little bit due to friction loss. As the flow hits the rotating rotor blades, the distribution of the total pressure in the leading edge region shows a small dip due to the incidence loss. The momentum transfer from the rotating blade to the flow between blades gives the rise in the total pressure inside the rotor passage. As the flow leaves the rotor and enters the stator, the total pressure of the flow starts to decrease slowly due to friction loss. Overall, the total pressure increases 38 percent as the flow passes from the inlet of the IGV to the outlet of the stator of the first stage.

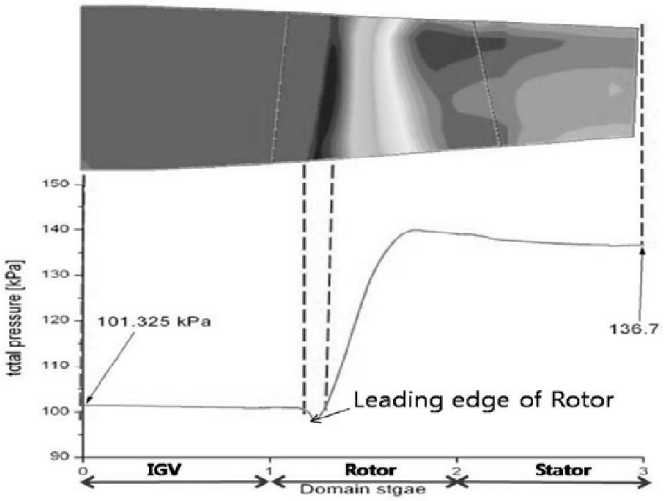

Figure 7 Averaged total pressure of the compressor with IGV

Figure 8 shows the computed distribution of static pressure on the plane located at 90% span of the IGV, rotor and stator. The static pressure shows gradual and smooth variation in the IGV region while it displays rapid variation inside the rotor passage. The rapid variation near the leading edge is mainly due to the formation of the stagnation point. As the pressure side of the blade shows relatively higher value and smooth variation of the static pressure, the suction side of the blade shows relatively low value and steep variation of the static pressure. The dense contour lines near the 70% chord of the suction surface indicate the formation of the normal shock. The pressure variation in the stator region is similar to that in the rotor region except there is no normal shock in the stator region.

Figure 9 shows the distribution of the static pressure averaged over planes perpendicular to the axis. The steady-state solution gives 90kPa for the static pressure at the inlet of the domain, which is interesting when the total pressure of 101kPa was specified at the inlet as the boundary condition of the CFD computation. The difference between the total pressure and the static pressure must have been converted to the dynamic pressure corresponding to the mass flow rate at the design point. The distribution of the static pressure shows much more variation compared to that of the total pressure, shown in

Figure 7, due to the acceleration and deceleration of the flow inside the flow passages.

Figure 10 shows the computed distribution of Mach number on the 90% span plane. The acceleration of the flow can be observed in the suction side of the rotor and deceleration of the flow is found in the stator where the kinetic energy of the flow is conserved to the pressure energy. A supersonic pocket is formed on the front part of the suction surface of the rotor, which is followed by a normal shock near the 70% chord.

Figures 11 shows the distribution of the Mach number averaged over planes perpendicular to the axis. Some typical values of the Mach number are 0.42 at the inlet of the IGV, 0.50 at the outlet of the IGV, 0.68 inside the rotor, 0.72 in front of the stator, and 0.52 at the outlet of the stator.

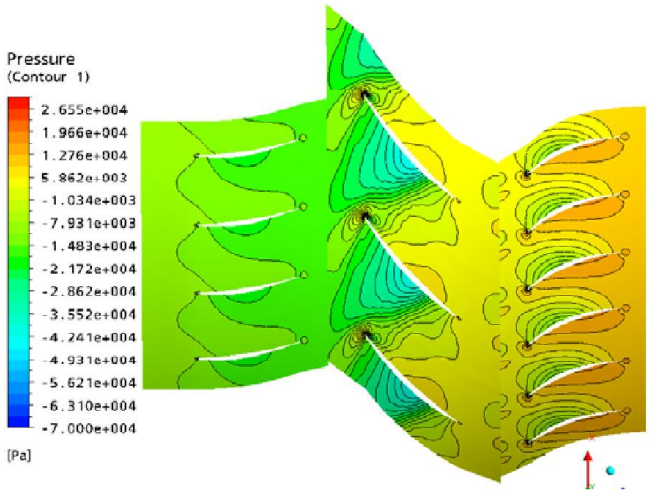

Figure 8 Static pressure contour at 90% span

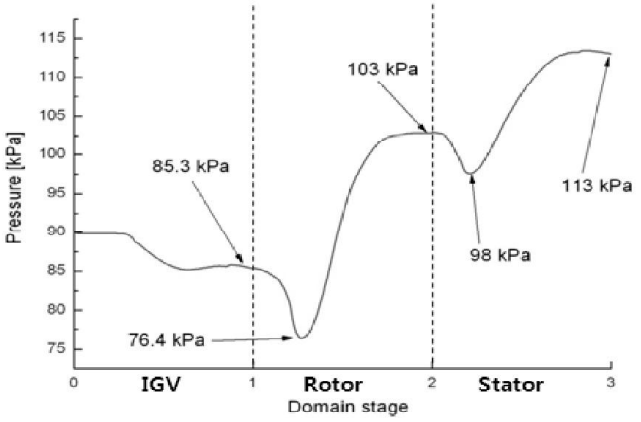

Figure 9 Averaged static pressure of the compressor

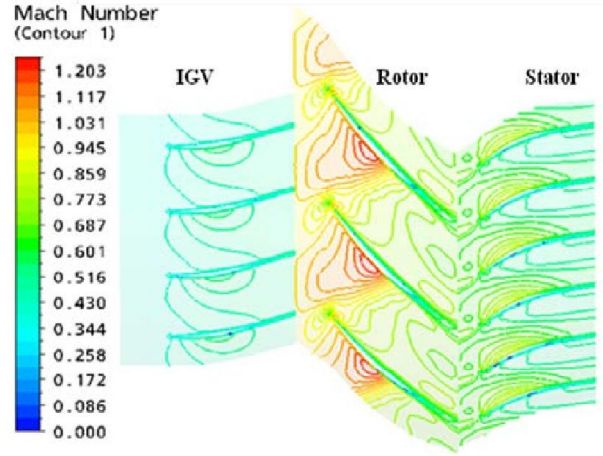

Figure 10 Mach number contour at 90% span

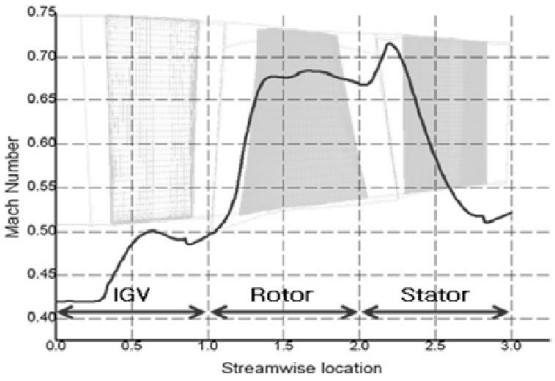

Figure 11 Averaged Mach number of the compressor

FSI ANALYSIS

As for the pre-step for the fully-coupled FSI calculation, a weakly-coupled FSI computation was conducted. The weakly-coupled FSI is also called one-way FSI which means that information flows in one direction, i.e. one way from aerodynamics to structural mechanics. Typical procedure of the weakly-coupled FSI is to obtain aerodynamic force from a steady CFD solution and then structural stress and deformation are obtained from the corresponding FEM solution by using the previously calculated aerodynamic force as input. Although the weakly FSI computation may not explain the nonlinear interaction of aerodynamics and structural mechanics, it provides a good starting point for a fully-coupled FSI study.

The rotor blade is made of Titanium and the material property of Titanium is listed in Table 3.

Figure 12 shows unstructured FEM mesh having 142,000 nodes and 130,000 elements. It is noted that the FEM grid points do not match with the CFD grid points at the interface of the rotor blade surface. The main difficulty of the FSI computation comes from the disagreement between the CFD mesh and the FEM mesh at the blade surface interface where information needs to be exchanged. ANSYS CFX 11.0 utilizes

MpCCI as the library for the information exchange at the interface of multi physics problems.

Table 3 Material properties of Titanium

Property	Value
Young`s Modulus	1.117+011 Pa
Poisson`s Ratio	0.3
Density	7850 kg/m^3
Thermal Expansion	1.2e-005 1/℃
Tensile Yield Strength	2.5e+008 Pa
Compressive Yield Strength	2.5e+008 Pa
Tensile Ultimate Strength	4.6e+008 Pa

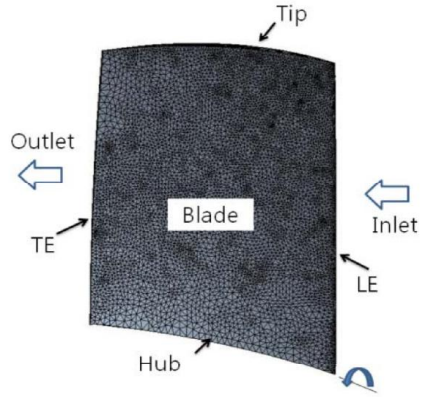

Figure 12 Surface mesh of the rotor blade for Weakly-coupled FSI analysis

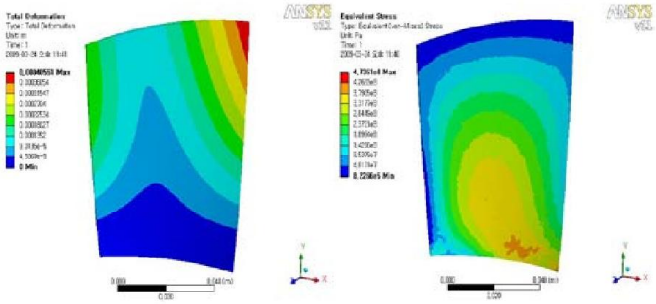

(a) Total deformation (b) Equivalent Stress(von-mises)

Figure 13 Weakly-coupled FSI solution of the rotor blade

Figure 13 shows the results of the weakly-coupled FSI solution for the calculated total deformation and equivalent (von-Mises) stress distribution indicating relatively high value in the lower center region of the rotor blade. The point of maximum stress of 4.74e08 Pa is located near the hub and toward the leading edge of the blade. The figure also shows that maximum total deformation occurs at the tip of the leading edge of the blade. Low part of the blade shows little deformation whereas relatively large deformation is observed in the tip region mainly due to high rotating speed.

Finally, a fully-coupled FSI computation was made after succeeding in obtaining the weakly-coupled FSI solution. Fully-coupled FSI is also called two-way FSI in which information flows in both directions, i.e. two way between aerodynamics and structural mechanics at every time step of the computation. Each time step of the fully-coupled FSI computation took about 424 CPU sec of a PC running in parallel mode on 20 CPUs, each with a clock speed of 3.2 GHz.

Two points were chosen to monitor the vibration history of the rotor blade. One of the points is located on the tip of the leading edge and the other point is on the tip of the trailing edge. Figure 14 shows the time history of the displacement of the two monitoring points as the fully-coupled FSI computation continues. The displacement shows stable periodic motion after passing unstable motion due to the sudden start of the FSI computation from the steady CFD solution. The displacement signal in the stable zone is zoomed and plotted again in Figure 15. It is clearly seen that the movement of the two monitoring points are in the same phase and they have the period of 0.0063 sec, i.e. the frequency of the vibration of the rotor tip is 159 Hz.

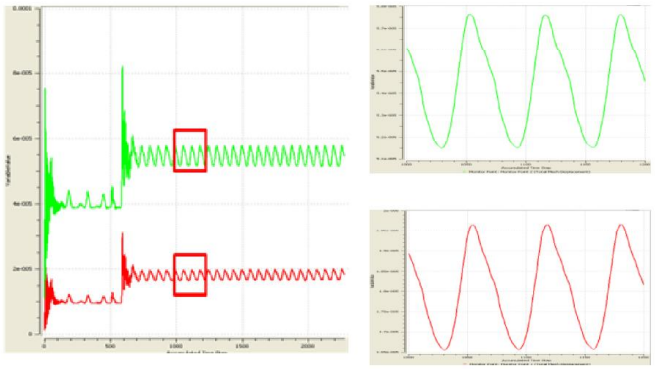

Figure 14 Time history of the displacement of the sampling points of the rotor

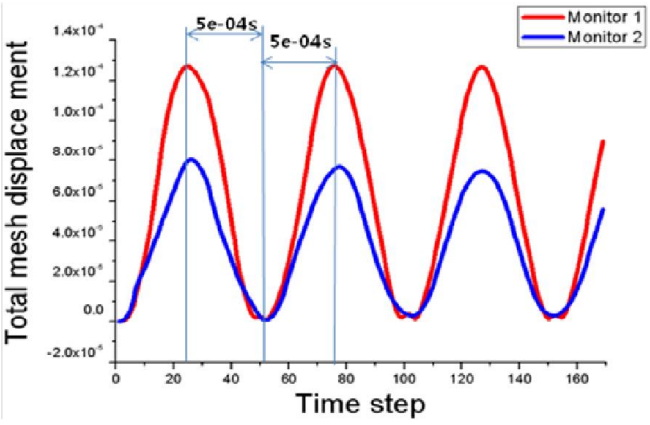

Figure 15 Total displacement of the leading edge and the trailing edge of the rotor tip

A Finite Element(FE) analysis has been made to find out fundamental vibration modes of the rotor blade in order to check the possibility of the resonance. The rotor blade is modelled with three-dimensional hexahedron solid element.

Figure 16 shows calculated vibration mode shapes of the rotor blade and Table 4 list the corresponding frequencies. The rotor has the first bending mode at 1,554 Hz which is quite high

compared to the flow induced vibration frequency of 159 Hz obtained from the fully-coupled FSI computation. So it is safe to conclude that the present compressor is free of flutter at design point operation.

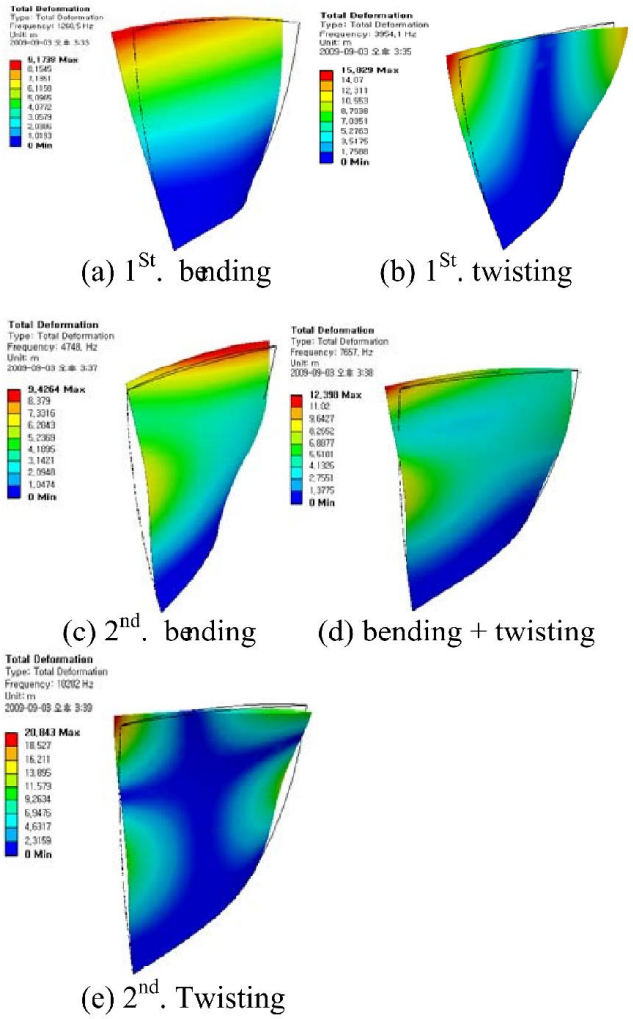

Figure 16 Mode shapes of rotor blade.

Table 4. Calculated frequencies of the vibration modes

Mode	Frequency[Hz]	Mode shape
1	1,554	Bending
2	4,540	Twisting
3	5,939	Bending
4	9,188	Bending+ Twisting
5	11,694	Twisting

CONCLUSION

A fully-coupled FSI computation has been made successfully by using ANSYS CFX-11 for the minimum flow passage model of the multi-stage transonic axial compressor with inlet guide vane. The frequency of the flow induced vibration is found out to be much lower than that of the first bending mode calculated from the separate FE analysis.

REFERENCES

[1] Ko, W.S., Kim, K.Y. and Ko, S.H., Aerodynamic Design optimization of A Transonic Axial Compressor Rotor with Readjustment of A Design Point, *Proceedings of the KFMA Annual Meeting 2003*, pp. 639-645.

[2] Chae, B.J. and Lee, S.W., Effects of Incidence Angle on the Three-Dimensional Flow and Aerodynamic Loss Downstream of a High-Turning Turbine Rotor Blade, *Proceedings of the KSME 2007 spring annual meeting*, 2007, pp. 440-445.

[3] Lakshminarayana, B., *Fluid Dynamics and heat Transfer of Turbomachinery*, John Wiley & Sons, New York, 1996.